Predicting the campbell soil water retention function

Comparing visible–near-infrared spectroscopy with classical pedotransfer function

Pittaki-Chrysodonta, Zampela; Moldrup, Per; Knadel, Maria; Iversen, Bo V.; Hermansen, Cecilie; Greve, Mogens H.; de Jonge, Lis Wollesen

Published in:
Vadose Zone Journal

DOI (link to publication from Publisher):
10.2136/vzj2017.09.0169

Publication date:
2018

Document Version
Publisher's PDF, also known as Version of record

Published May 3, 2018

Original Research

Core Ideas

- The Campbell model was anchored at a soil water content of −1000 cm H_2O matric potential.
- The two model parameters were predicted using either soil fines or vis–NIR spectroscopy.
- Both methods accurately predicted the soil water retention curve.

Predicting the Campbell Soil Water Retention Function: Comparing Visible–Near-Infrared Spectroscopy with Classical Pedotransfer Function

Zampela Pittaki-Chrysodonta,* Per Moldrup, Maria Knadel, Bo V. Iversen, Cecilie Hermansen, Mogens H. Greve, and Lis Wollesen de Jonge

The soil water retention curve (SWRC) is essential for the modeling of water flow and chemical transport in the vadose zone. The Campbell function and its *b* (pore-size distribution index) parameter fitted to measured data is a simple method to quantify retention under relatively moist conditions. Measuring soil water retention is time consuming, and a method to accurately predict the Campbell relation from either typically available soil parameters such as bulk density, clay-size fraction, and organic matter content (soil fines) or from visible–near-infrared (vis–NIR) spectroscopy may provide a fast and inexpensive alternative. However, the traditional Campbell model has a reference point at saturated water content, and this soil-structure-dependent water content will typically be poorly related to basic texture properties and thus be poorly predicted from vis–NIR spectra. In this study, we anchor the Campbell model at the water content at −1000 cm H_2O matric potential [log(1000)= pF 3]. Agricultural soil samples with a wide textural range from across Denmark were used. Soil water retention was measured at a number of matric potentials between pF 1 and 3. The soil water content at pF 3 and Campbell *b* were both well predicted using either a soil-fines-based pedotransfer function or vis–NIR spectroscopy. The resulting Campbell function anchored at pF 3 compared closely to measured water retention data for a majority of soils. The ability of the two methods to also predict field average SWRC was evaluated for three fields. Field average, predicted SWRC compared well with field average measured data, with vis–NIR overall performing better.

Abbreviations: CF, clay-size fraction; PLS, partial least squares; RMSEC, root mean square error of calibration; RMSECV, root mean square error of cross-validation; RPIQ, ratio of performance to interquartile distance; R^2Cal, coefficient of variation of the calibration dataset; R^2CV, coefficient of variation of the cross-validation dataset; OM, organic matter; SWRC, soil water retention curve; vis–NIR, visible–near-infrared.

Z. Pittaki-Chrysodonta, M. Knadel, B.V. Iversen, C. Hermansen, M.H. Greve, and L.W. de Jonge, Dep. of Agroecology, Faculty of Science and Technology, Aarhus Univ., Blichers Allé 20, PO Box 50, DK-8830 Tjele, Denmark; P. Moldrup, Dep. of Civil Engineering, Aalborg Univ., Thomas Manns Vej 23, DK-9220, Aalborg, Denmark. *Corresponding author (zambella.pittaki@agro.au.dk).

Received 13 Sept. 2017.
Accepted 13 Feb. 2018.

Citation: Pittaki-Chrysodonta, Z., P. Moldrup, M. Knadel, B.V. Iverson, C. Hermansen, M.H. Greve, and L.W. de Jonge. 2018. Predicting the Campbell soil water retention function: Comparing visible–near-infrared spectroscopy with classical pedotransfer function. Vadose Zone J. 17:170169. doi:10.2136/vzj2017.09.0169

The soil water retention curve (SWRC), which relates the soil water content and matric potential, is important for understanding water and solute movement in the vadose zone and water availability for plants. However, measuring the SWRC in the laboratory is a highly time consuming and laborious process. During the last decades, several mechanistic and empirical models for predicting the SWRC have been proposed (Brooks and Corey, 1964; Campbell, 1974; van Genuchten, 1980; Karup et al., 2017). The simplest model among these is the Campbell (1974) soil water retention function, only requiring a curve-shape parameter (the pore-size distribution parameter, *b*) and the saturated water content at the air-entry soil water potential as input. However, saturated water content is strongly related to soil structure and total porosity and less to texture (Jarvis et al., 1999; Babaeian et al., 2015). In addition, estimation of the air-entry soil water potential will often lead to erroneous water retention results, since there is a substantial variability of air-entry potential within textural classes (Clapp and Hornberger, 1978). To avoid these problems, we suggest anchoring the Campbell soil water retention function not at air-entry, but at a lower soil water potential (drier condition) where the corresponding soil water content is strongly related to soil texture.

In this study, we will use the water content at −1000 cm H_2O soil water matric potential (pF 3 [log(1000) = pF 3]) instead of saturated water content as a reference point. Hereby, the two only unknown parameters in the Campbell function become θ_{pF3} (volumetric water content at −1000 cm H_2O) and Campbell *b* (pore-size distribution index). For easy prediction of the SWRC, a fast and accurate method to predict these two parameters is needed.

Several pedotransfer functions have been developed to predict the SWRC on the basis of textural class or predicting water content at a given soil water potential from basic soil properties such as bulk density and clay- and sand-size fraction (Clapp and Hornberger, 1978; Gupta and Larson, 1979; Schaap et al., 1998). Clapp and Hornberger (1978) showed that Campbell *b* is a function of the clay-size fraction (CF), and Jensen et al. (2015) correlated the water content at different soil water potential with the texture, organic matter (OM) content, and bulk density. Although the implementation of pedotransfer functions is easy, the measurement of the required input data (e.g., clay content) is still fairly expensive.

During the last few decades, many attempts have been made to predict soil properties using spectroscopy due to its simplicity, rapidity, and low-cost analysis. Visible–near-infrared spectroscopy has previously been used successfully to predict soil attributes such as OM, clay content, fine silt content, the ratio between clay, and total organic C (Hermansen et al., 2016; Hermansen et al., 2017; Katuwal et al., 2018); soil structural properties (Katuwal et al., 2018); and complete particle size distribution (Hermansen et al., 2017). Few studies (Santra et al., 2009; Babaeian et al., 2015) have shown the ability of vis–NIR to predict the soil water retention curve. Babaeian et al. (2015) developed point and parametric spectral transfer functions to predict soil water contents at nine specific soil matric potentials (from saturation up to pF 4.2), as well as the parameters of van Genuchten (α and *n*) and Brooks–Corey (α and λ). Santra et al. (2009) used spectral transfer functions to predict the two parameters of van Genuchten water retention model α and *n* at wet parts (pF < 2.9). Furthermore, they related the spectral transfer function to the parameters of van Genuchten (α_{VG} and n_{VG}) and Brooks and Corey (α_{BC} and λ_{BC}) to predict these. To relate soil properties to spectral measurements, statistical methods are required to extract these properties, such as partial least squares (PLS) regression (Janik et al., 1998; Rossel et al., 2006; Nocita et al., 2011; Hermansen et al., 2016), principal component regression (Chang et al., 2001; Islam et al., 2003), or artificial neural networks (Rossel and Behrens, 2010).

The objective of this study was to examine if vis–NIR spectroscopy can perform equally well as a classical pedotransfer function to predict the SWRC. For that, vis–NIR models and soil-fines-based pedotransfer functions were developed using measured soil water retention curves for 219 undisturbed soil samples from Denmark, covering a wide range of soil textures, from sand to loam soils, and OM contents. Specifically, the two model parameters in the Campbell function anchored at pF 3, θ_{pF3} and Campbell *b*, were predicted using the two suggested methods. The first method (vis–NIR model) predicts the two parameters using vis–NIR calibration models. The second method (classical pedotransfer function) relates soil fines (i.e., CF and OM) and bulk density to θ_{pF3} and Campbell *b* using multiple linear regression. The two methods were compared, both for predicting the SWRC on individual soil samples and across-field variations.

Materials and Methods

Soil Samples

A total of 219 undisturbed 100-cm^3 (3.5-cm height, 6.1-cm diam.) core and bulk soil samples were used in this study. The samples were extracted from Danish agricultural fields comprising soils up to 20% (v/v) content of soil fines. The soil samples (soil core and bulk samples) were sampled from the 0- to 20-cm depth (topsoils) at different agricultural sites in Denmark: Silstrup (65 soil samples), Estrup (44), Jyndevad (87), Aarup (4), Saeby (9), and 10 soil samples from different localities in Denmark covering a variety of Danish soil types (Iversen et al., 2011). Three of the sites included in this study (Silstrup, Estrup, and Jyndevad) are part of the Danish Pesticide Leaching Assessment Program and are representative for agricultural soil types in Denmark. The soil samples from these three sites were taken in a grid with 15 m between grid points to represent across-field variations (Fig. 1). Detailed soil and site information about the Silstrup (56°55′ N, 8°38′ E), Jyndevad (54°53′ N, 9°07′ E), and Estrup (56°29′ N, 9°04′ E) sites can be found in Norgaard et al. (2013), Masís-Meléndez et al. (2014), and Paradelo et al. (2015), respectively.

Soil Characterization

The bulk soil samples were initially air dried and then 2-mm sieved. To determine the soil texture distribution, a combination of sieving and the hydrometer method was used (Gee and Or, 2002). Total organic C was determined on a Leco carbon analyzer coupled with an infrared CO_2 Flash 2000 NC detector (Thermo Fisher Scientific) and then was converted to OM by multiplying it by 1.72. After sampling, the soil cores were placed in sandboxes at −100 cm H_2O and then slowly saturated from below. The SWRC from pF 1 to 3 was measured for three replicates with sandboxes and the Richards pressure plate apparatus. Bulk density was determined for the 100-cm^3 core samples by oven drying at 105°C for 24 h. The soil samples were distributed across a large texture range from sand to loam soils (Fig. 1).

Campbell Retention Model Anchored at pF 3

A simple method to quantify the SWRC is the Campbell soil water retention function, which predicts the soil water matric potential (ψ) at a given volumetric water content (θ) anchored at the saturated volumetric water content (θ_s). The Campbell soil water retention model (Campbell, 1974) is expressed as

$$\psi = \psi_e \left(\frac{\theta}{\theta_s} \right)^{-b} \quad [1]$$

where ψ_e is the air-entry matric potential (cm H_2O). The empirical soil water retention parameter, Campbell *b*, is strongly dependent on soil texture (Clapp and Hornberger, 1978) and is regarded an index for the soil pore-size distribution (Moldrup et al., 2001). Campbell *b*

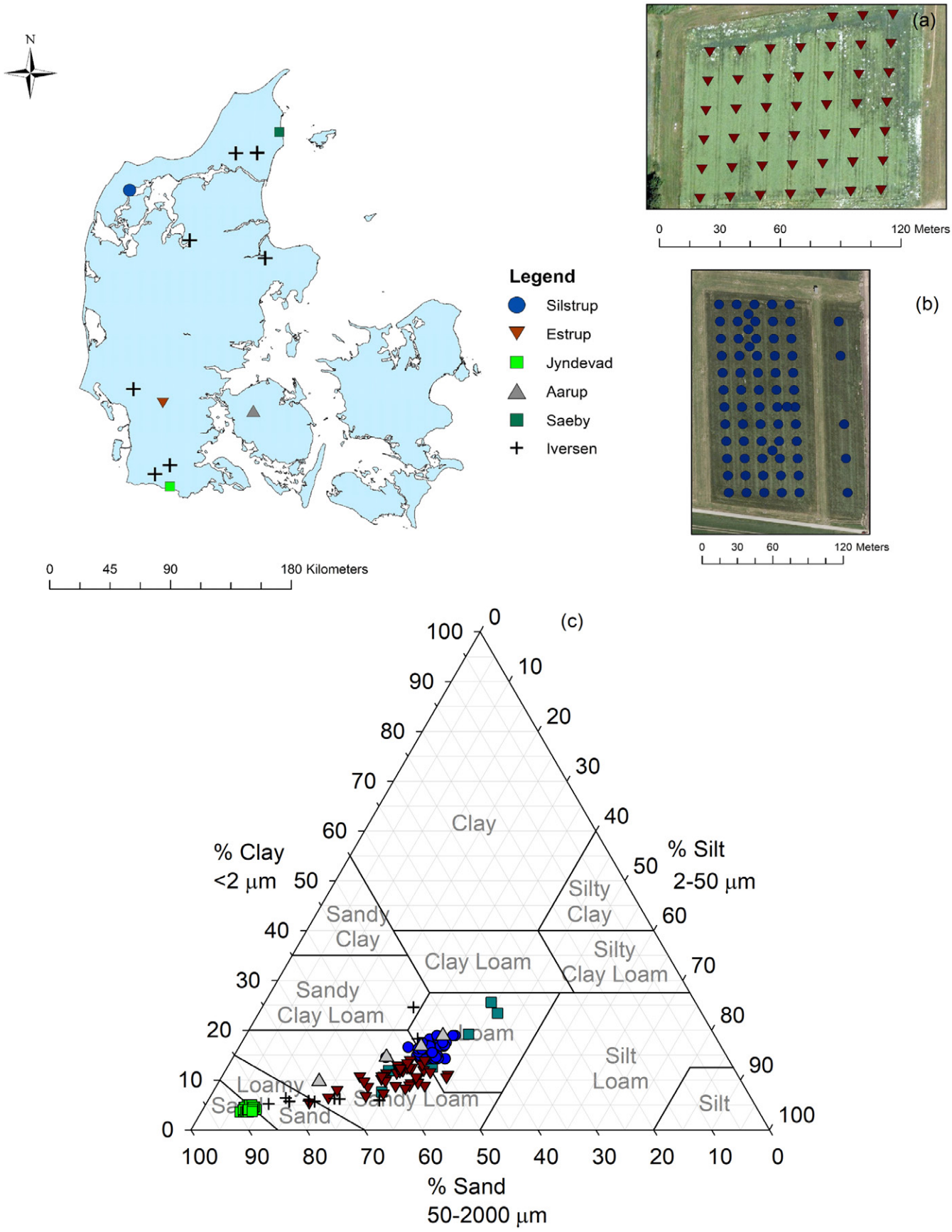

Fig. 1. Location of the agricultural fields and where soil samples were collected: sampling grid at (a) Estrup and (b) Silstrup; (c) distribution of the soil samples in the USDA soil texture triangle.

is equal to the slope of the SWRC on a log–log scale [log(−ψ) vs. log (θ) system]. Expressing the SWRC in log(−ψ) vs. log (θ) system yields

$$\log(-\psi) = -b\log(\theta) + E \quad [2]$$

where E is the intercept of the soil water retention in the log–log system. Equation [2] should produce a straight line (Campbell, 1974).

This study proposes anchoring the Campbell retention model, not at water saturation (θ_s), but with a reference point at the volumetric water content at −1000 cm H_2O soil water matric potential (pF 3). Anchoring the Campbell model (Eq. [1]) at pF 3, the new equation is expressed as

$$\psi = -1000\left(\frac{\theta}{\theta_{pF3}}\right)^{-b} \quad [3]$$

Examples of soil water retention measurements for a sand soil, sandy loam soil, and loam soil are illustrated in Fig. 2a. Furthermore, Fig. 2b shows the fitting of the original and the anchored Campbell soil water retention function for the measured soil water retention points of a loam soil.

Visible–Near-Infrared Spectroscopy

Approximately 50 g of the representative air-dried bulk soil sample was placed in a 60-mm sample cup, and the reflectance in the vis–NIR range (400–2500 nm) was measured with a NIRS DS2500 spectrometer (FOSS) with two detectors: Si (400–1100 nm) and PbS (1100–2500 nm). The spectral resolution was 0.5 nm. The reflectance measurements were transformed to absorbance by log(reflectance^{-1}). The reflectance was measured in seven positions, and the averaged spectrum was extracted for each soil sample.

Multivariate Data Analysis

Multivariate data analysis was performed using the PLS Toolbox 8.2 software (Eigenvector Research). All soil samples were included in the calibration model because some soil samples were derived either from a field or from a small sampling area at different locations (point samples). Measured data of Campbell b and θ_{pF3} were correlated with the spectral measurements using PLS regression analysis with the SIMPLS algorithm (de Jong, 1993). The models were validated using the venetian blind cross-validation method with 10 splits groups and one sample per split (Snee, 1977).

To find the best correlation between spectral data and reference data, spectra quality was improved by removing extraneous sources that are not important to the analysis, using different pretreatment techniques such as gap segment first and second derivative (Norris, 2001), Savitzky–Golay first and second derivative (Savitzky and Golay, 1964), standard normal variate transformation, and detrending (Barnes et al., 1989). The spectral data were mean centered.

For the statistical evaluation of the calibration models, the R^2, RMSE of calibration (RMSEC) and validation (RMSCV), and ratio of performance to interquartile distance (RPIQ) were used. The RMSEC is a measure of how well the model fits the data, whereas RMSECV is a measure of the ability of the model to determine the measured data (Campbell b and θ_{pF3}) that were not used to build the model. The RMSEC and RMSECV are defined as

$$\mathrm{RMSE} = \sqrt{\frac{1}{N}\sum_{i=1}^{N}\left(\widehat{y_i} - y_i\right)^2} \quad [4]$$

where N is the number of samples, $\widehat{y_i}$ is the predicted values, and y_i is the reference data.

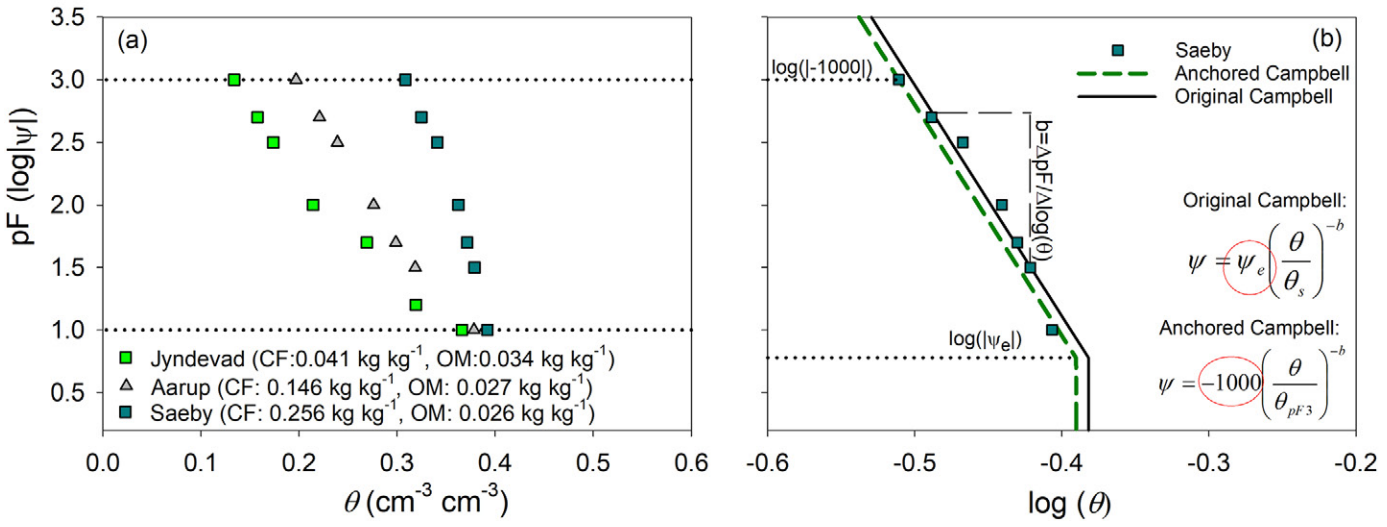

Fig. 2. (a) Examples of soil water retention measurements and the range of them (from pF 1 to 3) for three soils: a sand soil (Jyndevad), a sandy loam soil (Aarup), and a loam soil (Saeby). Clay-size fraction (CF) and organic matter (OM) content are also listed. (b) Schematic illustration for the calculation of the pore-size distribution index (Campbell b) for a soil sample (Saeby), as well as the fitting of the original Campbell and anchored Campbell function. ψ, soil water matric potential; θ, volumetric water content; ψ_e, air-entry matric potential; θ_s, saturated volumetric water content; θ_{pF3}, volumetric water content at −1000 cm H_2O.

The RPIQ represents the spread of the population regardless of the distribution (Bellon-Maurel et al., 2010). It is an index based on quartiles where Q_1 is the value below which 25% of the samples can be found and Q_3 is the value below which 75% of the samples can be found:

$$\mathrm{RPIQ} = \frac{\mathrm{IQ}}{\mathrm{SEP}} = \frac{Q_3 - Q_1}{\mathrm{SEP}} \quad [5]$$

where IQ is the interquartile distance and gives the range of dispersion around the median (or second quartile [Q_2]), and SEP is the SE of prediction. In this study, RMSECV is used instead of SEP.

The determination of the optimum number of factors (or latent variables) is crucial for the calibration of the model (Sileoni et al., 2013), since it is needed to maximize the amount of variation explained in spectral data that is relevant for predicting the reference data and also to not overestimate or underestimate the model. The optimum number of factors explaining the spectral matrix was identified by comparing RMCEC, RMSECV, and cumulative explained variance as a function of factors. Specifically, it is the local minimum value of the RMSEC and RMSECV that represents the most significant change in slope.

Soil-Fines-Based Pedotransfer Function

During the last few decades, many researchers have correlated the parameters of the SWRC with soil properties and developed several pedotransfer functions (Clapp and Hornberger, 1978; Saxton et al., 1986; Olesen et al., 2000; Jensen et al., 2015; Karup et al., 2016), since these properties (such as bulk density, CF, and OM) are easily available. Jensen et al. (2015) showed that the volumetric water content at pF 6 is related to the bulk density and clay, silt, and OM contents. Clapp and Hornberger (1978) provided a model for predicting Campbell *b* knowing only the CF. This study suggests using the following models to predict the anchored Campbell function at pF 3:

$$\theta_{\mathrm{pF3}} = A\rho_{\mathrm{d}}\left(\frac{\mathrm{CF}}{D_{\mathrm{p,s}}} + \frac{\mathrm{OM}}{D_{\mathrm{p,OM}}}\right) \quad [6]$$

and

$$b = B\rho_{\mathrm{d}}\left(\mathrm{CF} + \mathrm{OM}\right) \quad [7]$$

where ρ_{d} is bulk density (g cm^{-3}), CF is the clay-size fraction (kg kg^{-1}), OM is organic matter (kg kg^{-1}), $D_{\mathrm{p,s}}$ is the particle density of a soil sample (g cm^{-3}), $D_{\mathrm{p,OM}}$ is the particle density of OM (g cm^{-3}), and A and B are regression coefficients. The R^2, RPIQ, and RMSE were used for the evaluation of the soil-fines-based pedotransfer function.

Results and Discussion

Soil Properties

The statistical characteristics of the soil properties are presented in Table 1, and an overview of sampling locations and their distribution in the USDA texture triangle is illustrated in Fig. 1. A total of five different soil texture classes were observed. The CF and OM ranged from 0.036 to 0.256 and 0.017 to 0.126 kg kg^{-1}, respectively, whereas the bulk density ranged from 1.00 to 1.67 g cm^{-3}.

The soil sample texture ranged from sand to loam according to the USDA texture triangle. The Silstrup site is mostly characterized as loam, except for a few soil samples that were sandy loam. Jyndevad has a very narrow texture range with sand and loamy sand soils, whereas Estrup ranges from loamy sand to loam. The samples from Aarup and Saeby ranged from sandy loam to loam. Soil samples from Iversen have a wide texture range from sand to sandy clay loam.

Volumetric water content at pF 3 varied between 0.084 (Jyndevad) and 0.319 kg kg^{-1} (Estrup), with average values for Silstrup, Estrup, and Jyndevad of 0.271, 0.252 and 0.106 kg kg^{-1}, respectively. The Kolmogorov–Smirnov statistic indicated that the θ_{pF3} values for the three fields were normally distributed at the 5% level of significance.

The values of Campbell *b*, which is an indicator of pore-size distribution, varied from 3.0 to 19.4. The Silstrup site has an average Campbell *b* value of 11.01 (loam soil), whereas samples from Jyndevad have a lower value of 3.55 (sand and loamy sand soils). The Estrup soil has a wider texture range than the other two fields, and Campbell *b* ranged from 5.23 to 13.91, with an average value of 9.91.

Visible–Near-Infrared Measurements

Examples of raw absorption spectra for four soil samples: one spectrum each for low and high values of θ_{pF3} (sand and sandy loam soil, respectively), one spectrum for loamy sand soil (low value of Campbell *b*), and one spectrum for loam soil (high value of Campbell *b*) are shown in Fig. 3. The soil sample with the high θ_{pF3} (0.32 cm^3 cm^{-3}) value had clay, sand, and OM contents of 0.090, 0.577, and 0.104 kg kg^{-1}, respectively. For the sample with the low value (0.08 cm^3 cm^{-3}), the contents were 0.036, 0.894, and 0.027 kg kg^{-1}, respectively. The loam soil, which had a high value of Campbell *b* (19.35), had clay, sand, and OM contents of 0.234, 0.353 and 0.020 kg kg^{-1}, respectively. For the loamy sand soil with the low value (3.63), the contents were 0.057, 0.758 and 0.022 kg kg^{-1}, respectively. Therefore, the samples with the lowest values of θ_{pF3} and Campbell *b* represent low fine minerals and had higher absorbance throughout the vis–NIR range than the absorbance of the higher values (θ_{pF3} and Campbell *b*). The loamy sand and loam soils (low and high values of Campbell *b*) both had low OM contents, and therefore their absorption in the visible range was lower than that of the sand and sandy loam soils (low and high values of θ_{pF3}). Galvão and Vitorello (1998) have shown that, in the absence of organic C, reflectance increases through the vis–NIR range, especially in the range from 600 to 750 nm and therefore absorption in this range is decreased. The peaks near 1400 and 1900 nm indicate the presence of water molecules, and if molecular water is present, these two features always appear (Hunt, 1977). The peak at 2200 nm appears because of the combination of the OH stretch with the fundamental Al-OH bending mode (Hunt, 1977).

Table 1. General statistics of the investigated soil properties and the datasets.

Dataset	Statistic†	Soil property‡				
		CF	OM	ρ_d	θ_{pF3}	Campbell *b*
		kg kg^{-1}		g cm^{-3}	cm^3 cm^{-3}	
Silstrup (*N* = 65)	Mean	0.159	0.034	1.451	0.271	11.01
	Median	0.156	0.034	1.461	0.272	10.81
	Q_1	0.149	0.033	1.407	0.266	10.03
	Q_3	0.168	0.035	1.495	0.279	11.91
	σ	0.013	0.002	0.063	0.011	1.50
	Min.–max.	0.142–0.189	0.029–0.038	1.275–1.555	0.239–0.294	8.14–15.95
Estrup (*N* = 44)	Mean	0.108	0.053	1.360	0.252	9.91
	Median	0.108	0.044	1.375	0.254	9.88
	Q_1	0.095	0.037	1.303	0.232	8.49
	Q_3	0.124	0.061	1.447	0.267	11.40
	σ	0.021	0.023	0.117	0.030	2.03
	Min.–max.	0.055–0.246	0.031–0.126	1.070–1.534	0.172–0.319	5.23–13.91
Jyndevad (*N* = 87)	Mean	0.042	0.031	1.416	0.106	3.55
	Median	0.041	0.031	1.410	0.104	3.45
	Q_1	0.040	0.029	1.386	0.098	3.30
	Q_3	0.045	0.034	1.441	0.112	3.69
	σ	0.004	0.004	0.049	0.011	0.34
	Min.–max.	0.036–0.050	0.024–0.043	1.291–1.577	0.084–0.134	3.04–4.63
Aarup (*N* = 4)	Mean	0.150	0.029	1.328	0.214	8.82
	Median	0.157	0.030	1.310	0.219	8.67
	Q_1	0.134	0.026	1.284	0.183	6.51
	Q_3	0.173	0.033	1.353	0.249	10.97
	σ	0.039	0.006	0.075	0.057	4.00
	Min.–max.	0.097–0.189	0.021–0.033	1.260–1.432	0.143–0.276	4.27–13.65
Saeby (*N* = 9)	Mean	0.167	0.022	1.554	0.258	14.63
	Median	0.175	0.022	1.560	0.258	15.31
	Q_1	0.126	0.019	1.515	0.230	11.92
	Q_3	0.192	0.024	1.606	0.284	17.88
	σ	0.057	0.003	0.082	0.034	4.04
	Min.–max.	0.076–0.256	0.017–0.028	1.389–1.666	0.209–0.308	6.98–19.35
Iversen (*N* = 10)	Mean	0.090	0.030	1.386	0.179	6.64
	Median	0.060	0.029	1.421	0.164	4.42
	Q_1	0.057	0.027	1.362	0.137	3.65
	Q_3	0.064	0.032	1.443	0.190	5.50
	σ	0.067	0.008	0.151	0.060	5.26
	Min.–max.	0.052–0.246	[0.022–0.049]	1.00–1.544	0.116–0.282	3.50–18.53
Total (*N* = 219)	Mean	0.099	0.036	1.419	0.197	7.78
	Median	0.097	0.033	1.420	0.230	8.44
	Q_1	0.045	0.030	1.381	0.108	3.58
	Q_3	0.149	0.036	1.470	0.270	10.83
	σ	0.056	0.014	0.090	0.079	4.08
	Min.–max.	0.036–0.256	0.017–0.126	1.000–1.666	0.084–0.319	3.04–19.35

† Q_1, first quartile of the dataset; Q_3, third quartile of the dataset.
‡CF, clay-size fraction; OM, organic matter; ρ_d, bulk density; θ_{pF3}, volumetric water content at –1000 H_2O; Campbell *b*, pore-size distribution index.

Partial Least Squares Regression Analysis

The pretreatment method, Savitzky–Golay second derivative, was applied to the vis–NIR spectra, as this method resulted in the best calibration models of the tested pretreatment methods. Figure 4 shows the optimum number of factors selected for each model, according to the RMSEC, RMSECV, and cumulative explained variance as a function of factors. The optimum number of factors was five for both models. The results of the PLS regression analysis for the models are presented in Table 2. Specifically, the predictions of θ_{pF3} and Campbell *b* yielded an R^2 of 0.93 and 0.86 and RMSE of 0.022 and 1.519, respectively. Furthermore, the value of RPIQ indicates that the model for θ_{pF3} performed better than the

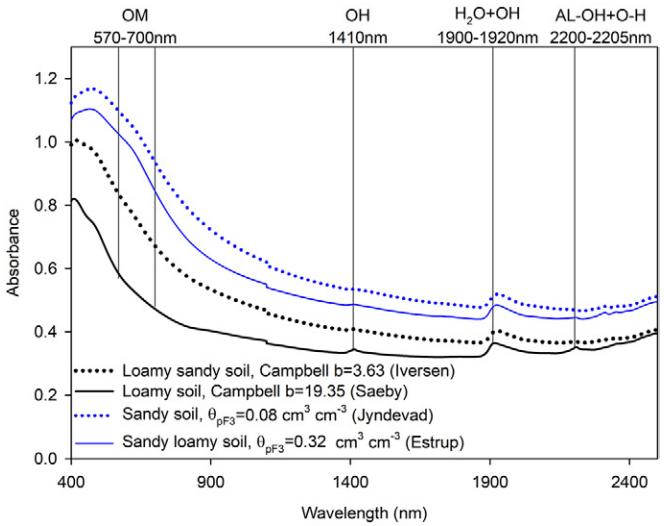

Fig. 3. Visible–near-infrared spectra of the selected soil samples and the possible spectrally active components: for a loamy sand soil and for a loam soil with low and high pore-size distribution index (Campbell *b*); and for a sand soil with a low value and sandy loam soil with a high volumetric water content at −1000 cm H_2O (θ_{pF3}). OM, organic matter.

model for Campbell *b*. Figure 5 compares values for Campbell *b* and θ_{pF3} predicted using vis–NIR against measured values. The statistical characteristics (mean, median Q_1, Q_3, σ, and range of θ_{pF3} and Campbell *b*) of the vis–NIR-predicted parameters using PLS regression for each dataset are presented in Table 3 and are close to the measured θ_{pF3}. The Q_1 values of the vis–NIR-predicted Campbell *b* were overpredicted from the measured values for the Aarup, Saeby,

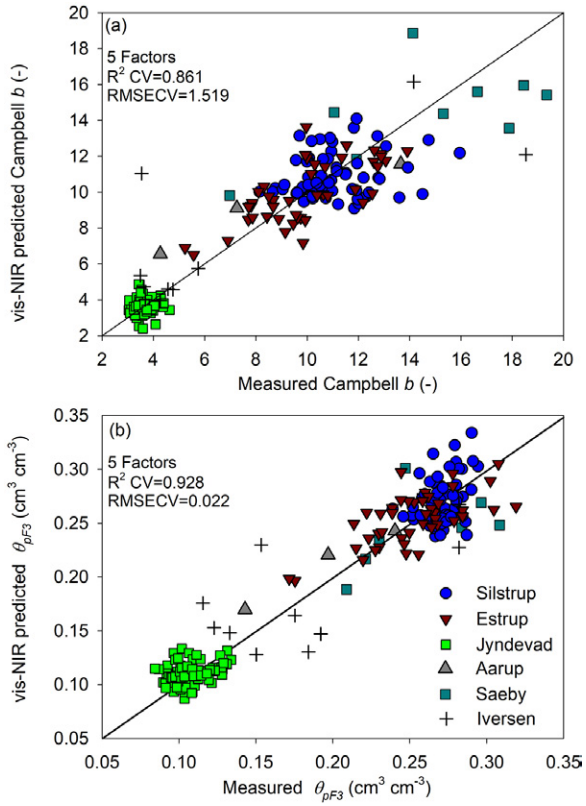

Fig. 5. Visible–near-infrared (vis–NIR) predicted vs. measured values of (a) pore-size distribution index (Campbell *b*) and (b) volumetric water content at −1000 cm H_2O (θ_{pF3}). Also given are the number of factors, R^2 of the cross-validation dataset (R^2CV), and the RMSE of cross-validation (RMSECV).

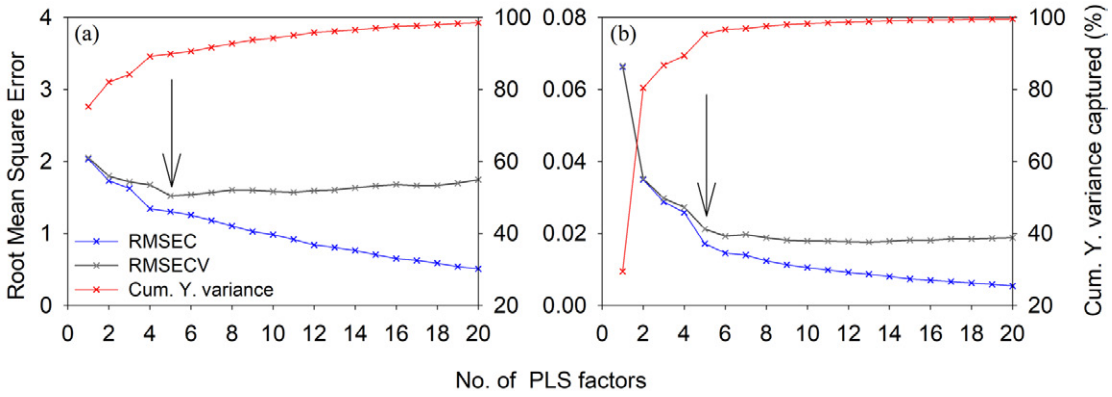

Fig. 4. Root mean square error of the calibration (RMSEC, blue line) and cross-validation (RMSECV, gray line) and cumulative *Y* variance (Cum. Y. variance) captured as a function of the number of factors in the partial least squares (PLS) regression. The arrow indicates the selected number of factors used in the models: (a) for pore-size distribution index and (b) for volumetric water content at −1000 cm H_2O.

Table 2. Partial least squares regression analysis of visible–near-infrared model.

		Parameter‡					
Parameter†	*N*	R^2Cal	R^2CV	RMSEC	RMSECV	RPIQ	Factors
θ_{pF3} (cm^3 cm^{-3})	219	0.95	0.92	0.017	0.022	6.80	5
Campbell *b*	219	0.90	0.86	1.3	1.519	4.62	5

† θ_{pF3}, volumetric water content at −1000 H_2O; Campbell *b*, pore-size distribution index.

‡ R^2Cal, R^2 of the calibration dataset; R^2CV, R^2 of cross-validation dataset; RMSEC, RMSE of the calibration dataset; RMSECV, RMSE of the cross-validation dataset; RPIQ, ratio of performance to interquartile distance.

and Iversen datasets (8.48, 13.57, and 4.57 instead of 6.51, 11.92 and 3.65, respectively). Furthermore, differences in Q_3 values were found in the Saeby and Iversen datasets (15.59 and 9.71 instead of 17.88 and 5.50, respectively). The slightly over- or underprediction of the specific soil samples may be related to the soil structure. Thus, larger number of macropores or interaggregate pores in the 100-cm^3 cores would lead to an overestimation, whereas a smaller number of macropores or intraaggregate pores would lead to an underestimation. Comparison of this study's results with the literature is of limited value, since not much research has been conducted in this area so far. However, Babaeian et al. (2015) developed spectral transfer functions using spectral reflectance values (from the vis–NIR range) as predictor variables and obtained lower R^2 values (0.53) for the prediction of θ_{pF3} than in this study. The higher R^2 value in this study may be related to the wider range of θ_{pF3} (0.084–0.319 kg kg^{-1}) than in the Babaeian et al. (2015) study (0.141–0.272 kg kg^{-1}).

Looking at Fig. 5, there is a trend toward bimodal data distribution, with Jyndevad and Silstrup representing relatively many points within a narrow interval of parameter values. To evaluate if this influenced the results, the entire analyses were repeated using only (i) 15 or (ii) 30 points for both Jyndevad and Siltrup fields (selected to represent the entire interval of Campbell *b* values for each soil). Strategies i and ii gave only minor changes in vis–NIR-based models and model performance for both Campbell *b* (R^2 of the calibration dataset [R^2Cal] = 0.89 and 0.90, R^2 of the cross-validation dataset [R^2CV] = 0.78 and 0.80 and RMSECV = 1.86 and 1.78 for i and ii, respectively) and θ_{pF3} (R^2Cal = 0.90 and 0.91, R^2CV = 0.87 and 0.88, and RMSECV = 0.024 and 0.024 for i and ii, respectively). The maximum deviation in R^2CV was 0.08, whereas the minimum was 0.05 between the models using 15, 30, and all points for the two fields.

Soil-Fines-Based Pedotransfer Function Analysis

The results from the multiple linear regression analysis for θ_{pF3} and Campbell *b* are presented in Table 4. The analysis showed that θ_{pF3} is linearly correlated with the volume of soil fines. The particle density of the CF was estimated to be 2.7 g cm^{-3}, which is close to the findings of other studies (Bielders et al., 1990; Blanco-Canqui et al., 2006; McBride et al., 2012; Schjønning et al., 2017), whereas the particle density of soil OM ranged between 0.9 and 1.3 g cm^{-3} and was assumed to be 1.0 g cm^{-3}. High values of R^2 and RPIQ (0.92 and 5.61) and a low value for RMSE (0.022 cm^3 cm^{-3}) resulted in a fairly good model. Rawls et al. (1982) performed a multiple linear regression analysis for the relationship between soil water content and soil fines (bulk density, sand, silt, clay, and OM), and the corresponding R^2

Table 3. Statistical characteristics of predicted parameters (volumetric water content at −1000 H_2O [θ_{pF3}] and pore-size distribution index [Campbell *b*]) for each dataset using the visible–near-infrared model.

Dataset	Parameter	Mean	Median	Q_1†	Q_3‡	σ	Min.–max.
Silstrup	θ_{pF3} (cm^3 cm^{-3})	0.269	0.263	0.253	0.282	0.023	0.234–0.334
	Campbell *b*	10.89	10.42	10.02	11.75	1.21	9.10–14.09
Estrup	θ_{pF3} (cm^3 cm^{-3})	0.254	0.259	0.239	0.269	0.024	0.197–0.305
	Campbell *b*	9.95	9.79	8.60	11.60	1.73	6.51–13.64
Jyndevad	θ_{pF3} (cm^3 cm^{-3})	0.109	0.109	0.101	0.115	0.010	0.087–0.133
	Campbell *b*	3.60	3.61	3.36	3.83	0.40	2.39–4.87
Aarup	θ_{pF3} (cm^3 cm^{-3})	0.223	0.232	0.208	0.247	0.039	0.170–0.259
	Campbell *b*	9.37	9.68	8.48	10.57	2.13	6.56–11.58
Saeby	θ_{pF3} (cm^3 cm^{-3})	0.247	0.248	0.234	0.269	0.033	0.188–0.301
	Campbell *b*	14.43	14.45	13.57	15.59	2.57	9.81–18.86
Iversen	θ_{pF3} (cm^3 cm^{-3})	0.177	0.158	0.147	0.214	0.048	0.128–0.267
	Campbell *b*	7.22	5.04	4.57	9.71	4.28	3.97–16.15
Total	θ_{pF3} (cm^3 cm^{-3})	0.196	0.234	0.113	0.262	0.077	0.087–0.334
	Campbell *b*	7.75	9.10	3.75	10.77	3.85	2.39–18.86

† Q_1, first quartile of the dataset.
‡ Q_3, third quartile of the dataset.

Table 4. Multiple linear regression analysis of the soil-fines-based pedotransfer function.

Parameter†	*N*	R^2	RMSE	Bias	RPIQ‡	Equation
θ_{pF3} (cm^3 cm^{-3})	219	0.92	0.0223	0.003	5.61	$1.94\rho_d\left(\frac{CF}{2.7}+\frac{OM}{1.00}\right)$
Campbell *b*	219	0.89	1.332	0.166	4.96	$41.13\rho_d(CF + OM)$

† θ_{pF3}, volumetric water content at −1000 H_2O; Campbell *b*, pore-size distribution index.
‡ RPIQ, ratio of performance to interquartile distance.

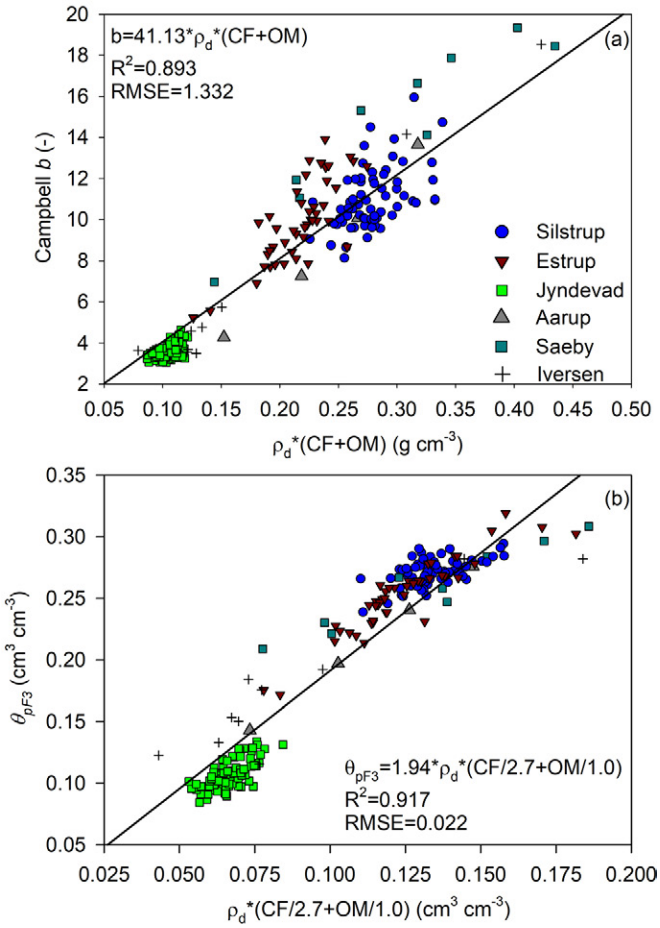

Fig. 6. Soil-fines-based pedotransfer functions for (a) pore-size distribution index (Campbell *b*) as a function of bulk density (ρ_d), clay-size fraction (CF), and organic matter (OM) and (b) volumetric water content at −1000 cm H_2O (θ_{pF3}) as a function of volumetric content of soil fines.

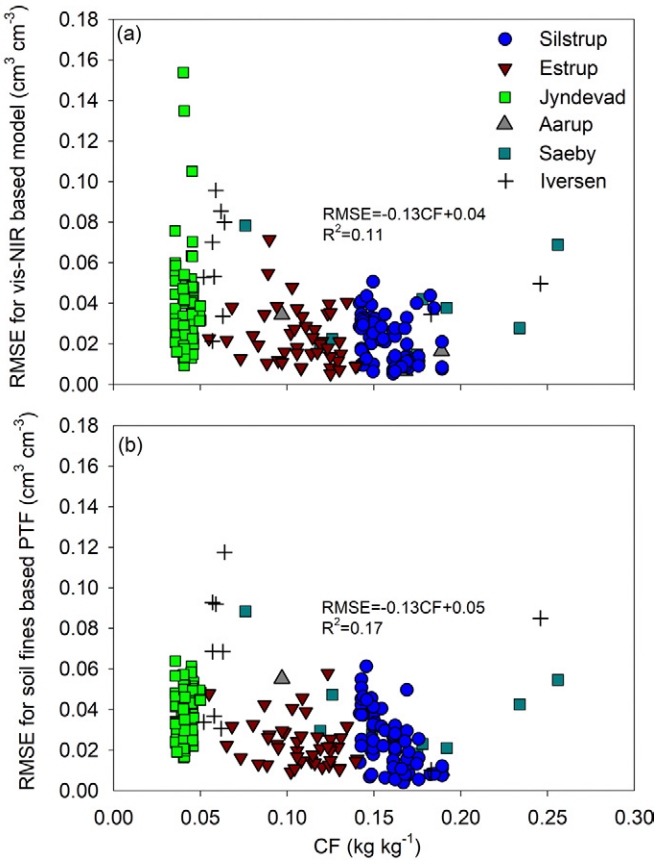

Fig. 7. Root mean square error in soil water content when predicting soil water retention from pF 1 to 3(pF = log|−ψ|, where ψ is the soil water matric potential). (a) Visible–near-infrared (vis–NIR) model and (b) soil-fines-based pedotransfer function (PTF) are shown as a function of clay-size fraction (CF).

Table 5. Statistical characteristics of predicted parameters (volumetric water content at −1000 H_2O [θ_{pF3}] and pore-size distribution index [Campbell *b*]) for each dataset using the soil-fines-based pedotransfer function.

Dataset	Parameter	Mean	Median	Q_1†	Q_3‡	σ	Min.–max.
Silstrup	θ_{pF3} ($cm^3\ cm^{-3}$)	0.260	0.257	0.250	0.271	0.019	0.213–0.306
	Campbell *b*	11.49	11.42	10.79	11.95	1.01	9.28–13.94
Estrup	θ_{pF3} ($cm^3\ cm^{-3}$)	0.241	0.231	0.221	0.258	0.038	0.151–0.352
	Campbell *b*	8.92	9.12	8.10	9.70	1.20	5.19–11.28
Jyndevad	θ_{pF3} ($cm^3\ cm^{-3}$)	0.129	0.128	0.120	0.136	0.012	0.103–0.163
	Campbell *b*	4.27	4.27	4.02	4.56	0.35	3.57–4.99
Aarup	θ_{pF3} ($cm^3\ cm^{-3}$)	0.218	0.222	0.185	0.255	0.062	0.142–0.286
	Campbell *b*	9.82	9.98	8.31	11.49	2.90	6.26–13.07
Saeby	θ_{pF3} ($cm^3\ cm^{-3}$)	0.255	0.266	0.195	0.295	0.069	0.150–0.360
	Campbell *b*	12.21	13.06	8.92	14.24	3.88	5.93–17.88
Iversen	θ_{pF3} ($cm^3\ cm^{-3}$)	0.174	0.145	0.132	0.179	0.083	0.084–0.356
	Campbell *b*	7.00	5.20	4.98	6.02	4.44	3.25–17.40
Total	θ_{pF3} ($cm^3\ cm^{-3}$)	0.199	0.216	0.131	0.256	0.068	0.084–0.360
	Campbell *b*	7.90	8.38	4.39	11.00	3.51	3.25–17.88

† Q_1, first quartile of the dataset.
‡ Q_3, third quartile of the dataset.

for θ_{pF3} was 0.76. Babaeian et al. (2015) related θ_{pF3} to the sand and C content, which yielded an R^2 value of 0.33 and a RMSE of 0.02 $cm^3\ cm^{-3}$.

Campbell *b* was strongly correlated with bulk density, CF, and OM, with R^2 and RPIQ values of 0.89 and 4.96, respectively, and a RMSE value of 1.33. When using the prediction method of Clapp and Hornberger (1978) (pedotransfer function based only on CF), Olesen et al. (1996) obtained an RMSE value of 1.75. Using the prediction method of Williams et al. (1989) (which correlates the Campbell *b* parameter with the CF, coarse sand, fine sand, and bulk density), the RMSE value was 1.67 for the same study. These correlations with the corresponding pedotransfer functions are illustrated in Fig. 6. The statistical characteristics (mean, median Q_1, Q_3, σ, and range of θ_{pF3} and Campbell *b*) of the predicted parameters using typically available soil fines for each dataset are presented in Table 5. The predicted mean values of θ_{pF3} are compared closely with the measurements for the majority of the soils, as well as the values of Campbell *b*. However, the predicted statistical characteristics of Campbell *b* for the Saeby database are underestimated and for the Aarup and Iversen datasets are overestimated.

Comparison of Visible–Near-Infrared Model and Soil-Fines-Based Pedotransfer Function

The two parameters (θ_{pF3} and Campbell *b*) obtained using the two methods were inserted into the anchored Campbell function, and the ability to predict SWRC was tested. The RMSE in soil water content when predicting soil water retention from pF 1 to 3 (using either vis–NIR or soil-fines-based pedotransfer function) for each soil sample is presented as a function of CF in Fig. 7. The RMSE had very weak correlation with CF for both methods (R^2 = 0.11 and 0.17 for vis–NIR and soil-fines-based pedotransfer function, respectively).

Figure 8 depicts an example of the performance of SWRC for 12 soil samples (two representative soil samples for the Aarup, Saeby, Iversen, Silstrup, Estrup, and Jydevad datasets). Soil-fines-based pedotransfer function showed slightly better predictions for five soils (one soil each from Aarup, Saeby, Estrup, and Jyndevad and two soils from Iversen), whereas the vis–NIR model presented better predictions for three soils (one soil each from Saeby, Silstrup, and Jyndevad). The remaining four soils were predicted equally well by both methods.

The ability to predict SWRC across-field variations (using three available field datasets) was also tested using the mean values of Campbell *b* and θ_{pF3} of each field predicted by the vis–NIR

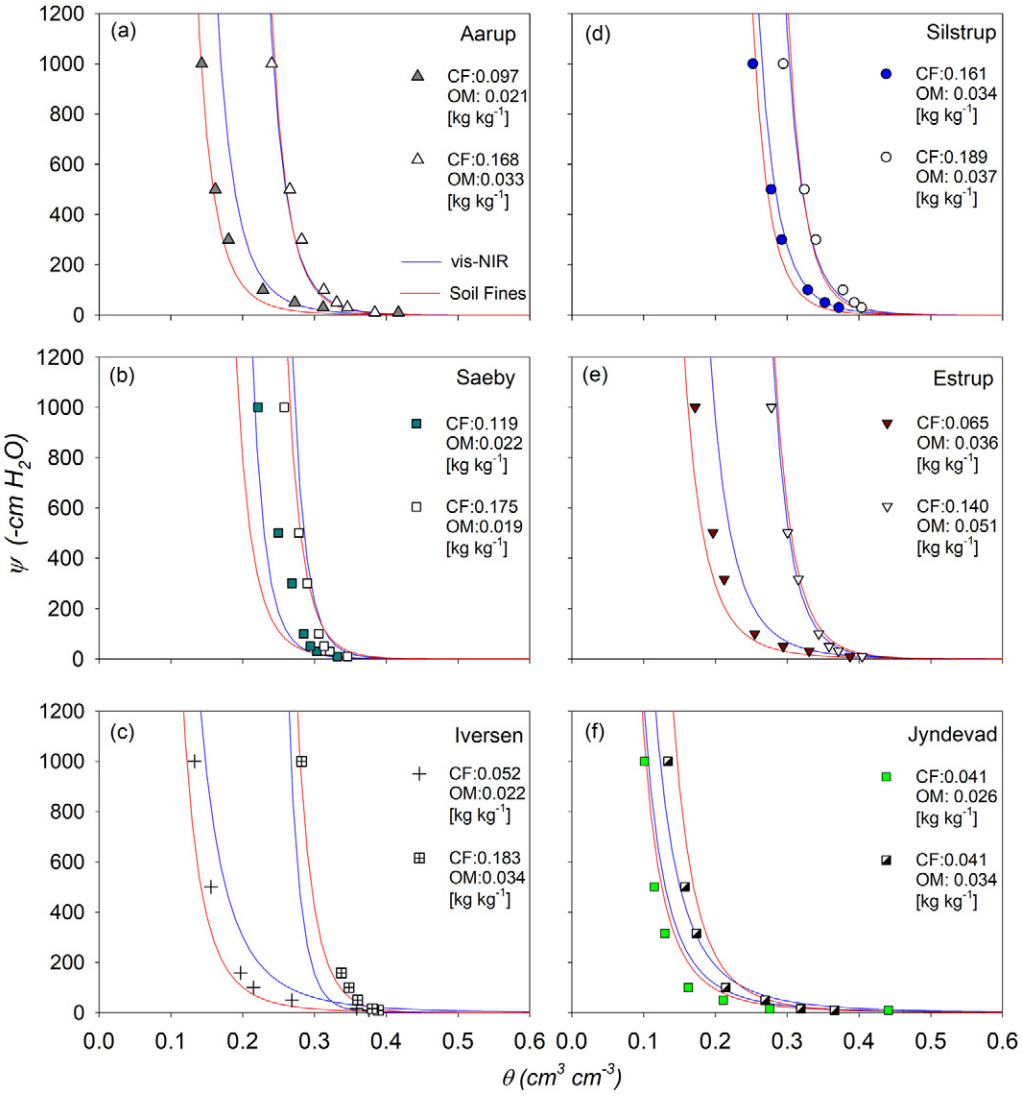

Fig. 8. Examples of predictive performance of soil water retention curve using the visible–near-infrared (vis–NIR) model and soil-fines-based pedotransfer function for 12 soil samples, two soils each from (a) Aarup, (b) Saeby, (c) Iversen, (d) Silstrup, (e) Estrup, and (f) Jyndevad. CF, clay-size fraction; OM, organic matter; ψ, soil water matric potential; θ, volumetric water content.

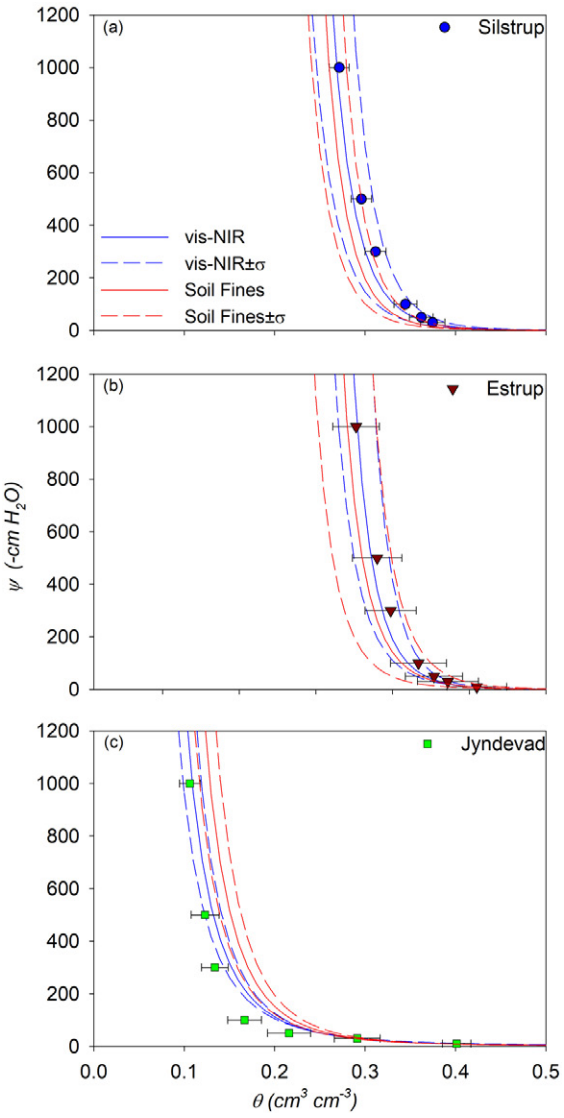

Fig. 9. Comparison of average measurements of soil water retention points and soil water retention data curves using visible–near-infrared (vis–NIR) model and soil-fines-based pedotransfer function for the three fields: (a) Silstrup, (b) Estrup, and (c) Jyndevad. Dashed lines indicate the possible predicted range (average ± σ). Soil water matric potential (ψ) is shown on the *y*-axis and volumetric water content (θ) is shown on the *x*-axis.

model or soil-fines-based pedotransfer function, and the results are shown in Fig. 9. For Silstrup and Estrup, the average measurements of soil water retention points and soil water retention data curves were slightly better using predictions from the vis–NIR model, rather than the soil-fines-based pedotransfer function. For Jyndevad, which has lower ranges of soil water retention data, the predictive ability of the soil-fines-based pedotransfer function was poorer than that of the vis–NIR model.

Conclusions

This study presents two methods for predicting the SWRC for a wide range of soil textures and OM contents: using either vis–NIR measurements or typically available soil fines. The Campbell soil water retention function was anchored not at saturation but at pF 3, and the two model parameters predicted were θ_{pF3} and Campbell *b*.

Given the RPIQ, the model of θ_{pF3} using vis–NIR spectroscopy was better than the model using a soil-fines-based pedotransfer function. However, for Campbell *b*, the soil-fines-based pedotransfer function was more accurate than the vis–NIR model. Furthermore, the two methods combined with the Campbell function anchored at pF 3 accurately predicted the SWRC across-field variations and for point soil samples. Both methods compared closely with the measured soil water retention data. However, the SWRC was slightly better predicted for point samples using the soil-fines-based pedotransfer function and across-field variations using the vis–NIR model.

Although both models can be applied for a large texture range as a faster and indirect method to predict the SWRC across-field variations or for point soil samples, the present study comprises soils up to 20% (v/v) content of fines, and subsequent studies should also include highly clay soils (with >20% fines content). Furthermore, data from broader texture classes, as well as from different geographical locations, should be added to these models to extend the capability of the models.

Acknowledgments

This research was funded by the Aarhus University Research Foundation (Grant AUFF-E-2016-9-36).

References

Babaeian, E., M. Homaee, H. Vereecken, C. Montzka, A.A. Norouzi, and M.Th. van Genuchten. 2015. A comparative study of multiple approaches for predicting the soil–water retention curve: Hyperspectral information vs. basic soil properties. Soil Sci. Soc. Am. J. 79:1043–1058. doi:10.2136/sssaj2014.09.0355

Barnes, R.J., M.S. Dhanoa, and S.J. Lister. 1989. Standard normal variate transformation and de-trending of near-infrared diffuse reflectance spectra. Appl. Spectrosc. 43:772–777. doi:10.1366/0003702894202201

Bellon-Maurel, V., E. Fernandez-Ahumada, B. Palagos, J.M. Roger, and A. McBratney. 2010. Critical review of chemometric indicators commonly used for assessing the quality of the prediction of soil attributes by NIR spectroscopy. TrAC Trend Anal. Chem. 29:1073–1081. doi:10.1016/j.trac.2010.05.006

Bielders, C.L., L.W. Debacker, and B. Delvaux. 1990. Particle density of volcanic soils as measured with a gas pycnometer. Soil Sci. Soc. Am. J. 54:822–826. doi:10.2136/sssaj1990.03615995005400030034x

Blanco-Canqui, H., R. Lal, W.M. Post, R.C. Izaurralde, and M.J. Shipitalo. 2006. Organic carbon influences on soil particle density and rheological properties. Soil Sci. Soc. Am. J. 70:1407–1414. doi:10.2136/sssaj2005.0355

Brooks, R.H., and A.T. Corey. 1964. Hydraulic properties of porous media. Hydrol. Papers 3. Colorado State Univ., Fort Collins, CO.

Campbell, G.S. 1974. Simple method for determining unsaturated conductivity from moisture retention data. Soil Sci. 117:311–314. doi:10.1097/00010694-197406000-00001

Chang, C.W., D.A. Laird, M.J. Mausbach, and C.R. Hurburgh. 2001. Near-infrared reflectance spectroscopy–principal components regression analyses of soil properties. Soil Sci. Soc. Am. J. 65:480–490. doi:10.2136/sssaj2001.652480x

Clapp, R.B., and G.M. Hornberger. 1978. Empirical equations for some soil hydraulic properties. Water Resour. Res. 14:601–604. doi:10.1029/WR014i004p00601

de Jong, S. 1993. Simpls: An alternative approach to partial least-squares regression. Chemom. Intell. Lab. Syst. 18:251–263. doi:10.1016/0169-7439(93)85002-X

Galvão, L.S., and I. Vitorello. 1998. Variability of laboratory measured

soil lines of soils from southeastern Brazil. Remote Sens. Environ. 63:166–181. doi:10.1016/S0034-4257(97)00135-1

Gee, G.W., and D. Or. 2002. Particle-size analysis. In: J.H. Dane and C.G. Topp, editors, Methods of soil analysis. Part 4. Physical methods. SSSA Book Ser. 5. SSSA, Madison, WI. p. 255–293. doi:10.2136/sssabookser5.4.c12

Gupta, S.C., and W.E. Larson. 1979. Estimating soil water retention characteristics from particle-size distribution, organic matter percent, and bulk density. Water Resour. Res. 15:1633–1635. doi:10.1029/WR015i006p01633

Hermansen, C., M. Knadel, P. Moldrup, M.H. Greve, R. Gislum, and L.W. de Jonge. 2016. Visible–near-infrared spectroscopy can predict the clay/organic carbon and mineral fines/organic carbon ratios. Soil Sci. Soc. Am. J. 80:1486–1495. doi:10.2136/sssaj2016.05.0159

Hermansen, C., M. Knadel, P. Moldrup, M.H. Greve, D. Karup, and L.W. de Jonge. 2017. Complete soil texture is accurately predicted by visible near-infrared spectroscopy. Soil Sci. Soc. Am. J. doi:10.2136/sssaj2017.02.0066

Hunt, G.R. 1977. Spectral signatures of particulate minerals in visible and near infrared. Geophysics 42:501–513. doi:10.1190/1.1440721

Islam, K., B. Singh, and A. McBratney. 2003. Simultaneous estimation of several soil properties by ultra-violet, visible, and near-infrared reflectance spectroscopy. Aust. J. Soil Res. 41:1101–1114. doi:10.1071/SR02137

Iversen, B.V., C.D. Borgesen, M. Laegdsmand, M.H. Greve, G. Heckrath, and C. Kjaergaard. 2011. Risk predicting of macropore flow using pedotransfer functions, textural maps, and modeling. Vadose Zone J. 10:1185–1195. doi:10.2136/vzj2010.0140

Janik, L.J., R.H. Merry, and J.O. Skjemstad. 1998. Can mid infrared diffuse reflectance analysis replace soil extractions? Aust. J. Exp. Agric. 38:681–696. doi:10.1071/EA97144

Jarvis, N.J., I. Messing, M.H. Larsson, and L. Zavattaro. 1999. Measurement and prediction of near-saturated hydraulic conductivity for use in dual-porosity models. In: M.Th. van Genuchten et al., editors, Characterization and measurement of the hydraulic properties of unsaturated porous media: Proceedings of the International Workshop on Characterization and Measurement of the Hydraulic Properties of Unsaturated Porous Media, Riverside, CA. 22–24 Oct. 1997. Univ. of California, Riverside. p. 839– 850.

Jensen, D.K., M. Tuller, L.W. de Jonge, E. Arthur, and P. Moldrup. 2015. A new two-stage approach to predicting the soil water characteristic from saturation to oven-dryness. J. Hydrol. 521:498–507. doi:10.1016/j.jhydrol.2014.12.018

Karup, D., P. Moldrup, M. Paradelo, S. Katuwal, T. Norgaard, M.H. Greve, and L.W. de Jonge. 2016. Water and solute transport in agricultural soils predicted by volumetric clay and silt contents. J. Contam. Hydrol. 192:194–202. doi:10.1016/j.jconhyd.2016.08.001

Karup, D., P. Moldrup, M. Tuller, E. Arthur, and L.W. de Jonge. 2017. Prediction of the soil water retention curve for structured soil from saturation to oven-dryness. Eur. J. Soil Sci. 68:57–65. doi:10.1111/ejss.12401

Katuwal, S., C. Hermansen, M. Knadel, P. Moldrup, M.H. Greve, and L.W. de Jonge. 2018. Combining X-ray computed tomography and visible near-infrared spectroscopy for prediction of soil structural properties. Vadose Zone J. 17:160054. doi:10.2136/vzj2016.06.0054

Masís-Meléndez, F., T.K.K. Chamindu Deepagoda, L.W. de Jonge, M. Tuller, and P. Moldrup. 2014. Gas diffusion-derived tortuosity governs saturated hydraulic conductivity in sandy soils. J. Hydrol. 512:388–396. doi:10.1016/j.jhydrol.2014.02.063

McBride, R.A., R.L. Slessor, and P.J. Joosse. 2012. Estimating the particle density of clay-rich soils with diverse mineralogy. Soil Sci. Soc. Am. J. 76:569–574. doi:10.2136/sssaj2011.0177n

Moldrup, P., T. Olesen, T. Komatsu, P. Schjønning, and D.E. Rolston. 2001. Tortuosity, diffusivity, and permeability in the soil liquid and gaseous phases. Soil Sci. Soc. Am. J. 65:613–623. doi:10.2136/sssaj2001.653613x

Nocita, M., L. Kooistra, M. Bachmann, A. Muller, M. Powell, and S. Weel. 2011. Predictions of soil surface and topsoil organic carbon content through the use of laboratory and field spectroscopy in the Albany Thicket Biome of Eastern Cape Province of South Africa. Geoderma 167–168:295–302. doi:10.1016/j.geoderma.2011.09.018

Norgaard, T., P. Moldrup, P. Olsen, A.L. Vendelboe, B.V. Iversen, M.H. Greve, et al. 2013. Comparative mapping of soil physical–chemical and structural parameters at field scale to identify zones of enhanced leaching risk. J. Environ. Qual. 42:271–283. doi:10.2134/jeq2012.0105

Norris, K. 2001. Applying Norris derivatives: Understanding and correcting the factors which affect diffuse transmittance spectra. NIR News 12:6–9. doi:10.1255/nirn.613

Olesen, T., P. Moldrup, K. Henriksen, and L.W. Petersen. 1996. Modeling diffusion and reaction in soils: IV. New models for predicting ion diffusivity. Soil Sci. 161:633–645. doi:10.1097/00010694-199610000-00001

Olesen, T., P. Moldrup, T. Yamaguchi, H.H. Nissen, and D.E. Rolston. 2000. Modified half-cell method for measuring the solute diffusion coefficient in undisturbed, unsaturated soil. Soil Sci. 165:835–840. doi:10.1097/00010694-200011000-00001

Paradelo, M., T. Norgaard, P. Moldrup, T.P.A. Ferré, K.G.I.D. Kumari, E. Arthur, and L.W. de Jonge. 2015. Prediction of the glyphosate sorption coefficient across two loamy agricultural fields. Geoderma 259–260:224–232. doi:10.1016/j.geoderma.2015.06.011

Rawls, W.J., D.L. Brakensiek, and K.E. Saxton. 1982. Estimation of soil water properties. Trans. ASAE 25:1316–1320. doi:10.13031/2013.33720

Rossel, R.A.V., and T. Behrens. 2010. Using data mining to model and interpret soil diffuse reflectance spectra. Geoderma 158:46–54. doi:10.1016/j.geoderma.2009.12.025

Rossel, R.A.V., D.J.J. Walvoort, A.B. McBratney, L.J. Janik, and J.O. Skjemstad. 2006. Visible, near infrared, mid infrared or combined diffuse reflectance spectroscopy for simultaneous assessment of various soil properties. Geoderma 131:59–75. doi:10.1016/j.geoderma.2005.03.007

Santra, P., R.N. Sahoo, B.S. Das, R.N. Samal, A.K. Pattanaik, and V.K. Gupta. 2009. Estimation of soil hydraulic properties using proximal spectral reflectance in visible, near-infrared, and shortwave-infrared (VIS–NIR–SWIR) region. Geoderma 152:338–349. doi:10.1016/j.geoderma.2009.07.001

Savitzky, A., and M.J.E. Golay. 1964. Smoothing and differentiation of data by simplified least squares procedures. Anal. Chem. 36:1627–1639. doi:10.1021/ac60214a047

Saxton, K.E., W.J. Rawls, J.S. Romberger, and R.I. Papendick. 1986. Estimating generalized soil-water characteristics from texture. Soil Sci. Soc. Am. J. 50:1031–1036. doi:10.2136/sssaj1986.03615995005000040039x

Schaap, M.G., F.J. Leij, and M.Th. van Genuchten. 1998. Neural network analysis for hierarchical prediction of soil hydraulic properties. Soil Sci. Soc. Am. J. 62:847–855. doi:10.2136/sssaj1998.03615995006200040001x

Schjønning, P., R.A. McBride, T. Keller, and P.B. Obour. 2017. Predicting soil particle density from clay and soil organic matter contents. Geoderma 286:83–87. doi:10.1016/j.geoderma.2016.10.020 [erratum: 292:150].

Sileoni, V., O. Marconi, G. Perretti, and P. Fantozzi. 2013. Evaluation of different validation strategies and long term effects in NIR calibration models. Food Chem. 141:2639–2648. doi:10.1016/j.foodchem.2013.04.110

Snee, R.D. 1977. Validation of regression models: Methods and examples. Technometrics 19:415–428. doi:10.1080/00401706.1977.10489581

van Genuchten, M.Th. 1980. A closed-form equation for predicting the hydraulic conductivity of unsaturated soils. Soil Sci. Soc. Am. J. 44:892–898. doi:10.2136/sssaj1980.03615995004400050002x

Williams, J., P. Ross, and K.L. Bristow. 1989. Prediction of the Campbell water retention function from texture, structure, and organic matter. In: M.Th. van Genuchten and F.J. Leij, editors, Proceedings of the International Workshop on Indirect Methods for Estimating the Hydraulic Properties of Unsaturated Soils, Riverside, CA. 11–13 Oct. 1989. Univ. of California, Riverside. p. 427–441.